A *bchD* (Magnesium Chelatase) Mutant of *Rhodobacter sphaeroides* Synthesizes Zinc Bacteriochlorophyll through Novel Zinc-containing Intermediates*

Paul R. Jaschke[‡], Amelia Hardjasa[‡], Elizabeth L. Digby[‡], C. Neil Hunter[§], and J. Thomas Beatty[‡1]

From the [‡]Department of Microbiology and Immunology, University of British Columbia, Vancouver V6T 1Z3, British Columbia, Canada and the [§]Department of Molecular Biology and Biotechnology, University of Sheffield, Sheffield S10 2TN, United Kingdom

Heme and bacteriochlorophyll *a* (BChl) biosyntheses share the same pathway to protoporphyrin IX, which then branches as follows. Fe^{2+} chelation into the macrocycle by ferrochelatase results in heme formation, and Mg^{2+} addition by Mg-chelatase commits the porphyrin to BChl synthesis. It was recently discovered that a *bchD* (Mg-chelatase) mutant of *Rhodobacter sphaeroides* produces an alternative BChl in which Mg^{2+} is substituted by Zn^{2+}. Zn-BChl has been found in only one other organism before, the acidophilic *Acidiphilium rubrum*. Our objectives in this work on the *bchD* mutant were to 1) elucidate the Zn-BChl biosynthetic pathway in this organism and 2) understand causes for the low amounts of Zn-BChl produced. The *bchD* mutant was found to contain a Zn-protoporphyrin IX pool, analogous to the Mg-protoporphyrin IX pool found in the wild type strain. Inhibition of ferrochelatase with *N*-methylprotoporphyrin IX caused Zn-protoporphyrin IX and Zn-BChl levels to *decline* by 80–90% in the *bchD* mutant, whereas in the wild type strain, Mg-protoporphyrin IX and Mg-BChl levels *increased* by 170–240%. Two early metabolites of the Zn-BChl pathway were isolated from the *bchD* mutant and identified as Zn-protoporphyrin IX monomethyl ester and divinyl-Zn-protochlorophyllide. Our data support a model in which ferrochelatase synthesizes Zn-protoporphyrin IX, and this metabolite is acted on by enzymes of the BChl pathway to produce Zn-BChl. Finally, the low amounts of Zn-BChl in the *bchD* mutant may be due, at least in part, to a bottleneck upstream of the step where divinyl-Zn-protochlorophyllide is converted to monovinyl-Zn-protochlorophyllide.

The purple non-sulfur bacterium *Rhodobacter sphaeroides* is a member of the α-proteobacteria and has become a model system for studying various aspects of photosynthesis, including bacteriochlorophyll *a* (BChl)[2] biosynthesis. The production of membrane-bound light-harvesting antenna and reaction center complexes (the photosystem) is repressed by high concentrations of oxygen and induced in response to low concentrations of oxygen (1). With a drop in oxygen levels, an intricate and highly coordinated response occurs as the organism shifts to anoxygenic phototrophic growth. The regulators PrrA-PrrB, AppA-PpsR, and FnrL sense changes in the oxygen tension, redox state of the electron transport chain, or light quality, which in turn cause a derepression of many genes involved in the synthesis of proteins, pigments, and membrane, which comprise the photosynthetic apparatus (2–5). The tetrapyrrole content of *R. sphaeroides* changes significantly upon a shift from aerobic to photosynthetic growth, with total tetrapyrroles increasing 200-fold (6).

The biosynthesis of tetrapyrroles begins with δ-aminolevulinic acid (ALA), which is converted through several enzymatic steps to protoporphyrin IX (PPIX) (7). The generation of ALA is a major regulatory point for downstream pathways. Studies of *R. sphaeroides* have indicated that there are two ALA synthase isoforms, encoded by *hemA* and *hemT*, which have separable kinetic properties and are differentially regulated (8–10). Oxygen represses ALA synthase transcription, but upon a lowering of oxygen levels, a 3–4-fold increase in *hemA* and *hemT* transcription occurs (11). Downstream products of the pathway appear to be important in post-transcriptional regulation because heme, magnesium protoporphyrin IX (Mg-PPIX), and PPIX have been shown to act as inhibitors of ALA synthase *in vitro*, although their relative importance *in vivo* remains unexplored (12, 13). A series of condensation reactions links ALA to PPIX. In photosynthetic organisms, PPIX lies at a major branch point: if PPIX is used as a substrate by ferrochelatase (HemH) to insert Fe^{2+}, heme is produced, whereas if PPIX is acted on by Mg-chelatase (BchHID) to insert Mg^{2+}, it is the first step in a long pathway leading to BChl.

In *R. sphaeroides*, ferrochelatase is a monomer and binds to the inner face of the cytoplasmic membrane, although there is a wide diversity of subunit composition and localization in different organisms (14). Transcript levels of the ferrochelatase gene appear to be relatively constant with changes in growth conditions, although a shift from aerobic respiratory to anaerobic photosynthetic growth resulted in a modest 2-fold increase in

[1] To whom correspondence should be addressed: Dept. of Microbiology and Immunology, 2350 Health Sciences Mall, Vancouver, British Columbia V6T 1Z3, Canada. Fax: 604-822-6041; E-mail: j.beatty@ubc.ca.

[2] The abbreviations used are: BChl, bacteriochlorophyll *a*; ALA, 5-aminolevulinic acid; DV, divinyl; MV, monovinyl; PChlide, protochlorophyllide; PPIX, protoporphyrin IX; MME, monomethyl ester; NMPP, *N*-methylprotoporphyrin IX.

heme levels (dwarfed by a 200-fold increase in total tetrapyrroles) (11, 15).

BchHID or a close homologue is found in all photosynthetic organisms and has been extensively studied (16–20). *In vitro* enzyme assays of *R. sphaeroides* Mg-chelatase showed that all three subunits are required for enzyme activity (17). The BchH subunit of Mg-chelatase binds PPIX tightly, and *Escherichia coli* cells that express *bchH* turn bright red from PPIX bound to BchH (17). The BchI and BchD proteins use ATP to generate a double ring protein structure that is believed to interact with the BchH-PPIX complex to transform PPIX to Mg-PPIX (21). After the formation of Mg-PPIX, eight enzymatic steps subsequently lead to the creation of BChl (reviewed in Refs. 22 and 23).

Recently, we discovered that a Mg-chelatase-deficient strain of *R. sphaeroides* containing a transposon-disrupted *bchD* gene (24) synthesizes zinc bacteriochlorophyll *a* (Zn-BChl) instead of the usual Mg-BChl found in wild type cells (25). The appearance of Zn-BChl in *R. sphaeroides* was surprising, because Zn-BChl had been found before only in the acidophilic purple bacterium *Acidiphilium rubrum.* Even more surprising was the fact that Zn-BChl biosynthesis in *A. rubrum* requires a functional Mg-chelatase (26), which the *R. sphaeroides bchD* mutant does not possess. Moreover, the *bchD* mutant did not produce Mg-BChl or bacteriopheophytin *a* (25), which are thought to be precursors of Zn-BChl in *A. rubrum*, such that Zn^{2+} is added "late" in the pathway (26, 27).

To explain how Zn-BChl is synthesized in the absence of both of the key intermediates used for Zn-BChl biosynthesis in *A. rubrum*, we hypothesized that the ferrochelatase enzyme produces zinc protoporphyrin IX (Zn-PPIX) in the *bchD* strain (25). The corollary of this "zinc-early" hypothesis is that the subsequent enzymes in the BChl biosynthetic pathway are able to use zinc-containing intermediates in place of magnesium-containing intermediates.

We present evidence here to show that the *bchD* mutant contains Zn-PPIX instead of Mg-PPIX and that the products of two subsequent BChl biosynthetic steps in the mutant contain Zn^{2+} instead of Mg^{2+}. Furthermore, ferrochelatase is shown to be necessary for Zn-PPIX and Zn-BChl biosynthesis. Our results support a model in which the *bchD* mutant synthesizes Zn-BChl through a novel variation of the BChl biosynthetic pathway that utilizes ferrochelatase in place of the Mg-chelatase as the first step in the pathway. Additionally, it appears that a bottleneck in the pathway leading to Zn-BChl is located upstream of the step where divinyl-Zn-protochlorophyllide is converted to monovinyl-Zn-protochlorophyllide.

EXPERIMENTAL PROCEDURES

Bacterial Strains and Culture Conditions—*R. sphaeroides* strains were cultivated at 30 °C in LB medium (28), containing neomycin at 20 μg/ml for the *bchD* mutant (TB59) (24) and lacking antibiotics for the wild type (NCIB8253). High to low aeration-shifted cultures were initially grown in flasks filled to 8% of the nominal volume on a rotary shaker at 300 rpm (high aeration) until exponential phase and then used to seed a flask filled to 80% of the nominal volume and shaken at 150 rpm (low aeration or semiaerobic growth).

Extraction of Porphyrins and BChls from Cells—Total porphyrins were extracted in three stages, essentially as described (29). Briefly, cell pellets were washed with 150 mM NaCl in 10 mM Tris-HCl (pH 8.0), followed by the addition of 1 ml of 9:1 acetone, 0.1 N NH_4OH (v/v) per 2 ml of culture with sonication at 4 °C. Cell debris was pelleted by centrifugation, and the resultant supernatant was extracted with an equal volume of hexane. The resulting hexane layer became orange or red with extracted carotenoids. This hexane extraction was repeated with ⅓ volume of hexane. To the remaining hexane-extracted acetone residue layer, ¹⁄₇₀ volume of 0.5 M KH_2PO_4 and ¹⁄₁₇ volume of saturated NaCl were added. To this mixture ⅕ volume of diethyl ether was added and mixed, with the resulting ether layer removed to a new tube and saved. The extraction was repeated 2–4 more times with ¹⁄₁₀ volume of ether, and all ether layers were pooled.

Extraction of heme from cell pellets was accomplished by resuspension of the cell pellet previously extracted as described above, in 80% acetone, and pelleting of particulate matter by centrifugation. The pellet of the 80% acetone wash was resuspended in 2% HCl (w/v) in acetone, followed by a final pelleting and removal of the acidified acetone supernatant, which contained heme (30).

N-Methylprotoporphyrin IX and Nicotinamide Inhibition—For inhibition of the ferrochelatase with *N*-methylprotoporphyrin IX, wild type and *bchD* mutant cultures were grown with high aeration until $A_{650} = 1.0$ and used to inoculate flasks filled to 80% of the nominal volume to $A_{650} = 0.2$. Simultaneously, filter-sterilized 1.8 mM *N*-methylprotoporphyrin IX stock (Frontier Scientific) dissolved in 20 mM NaOH, 2% Tween 20 (v/v) was added to a final concentration of 0.25, 0.50, 1.00, and 2.00 μM. The 0 μM condition had the same volume of solvent added as for the 2.0 μM condition but lacked *N*-methylprotoporphyrin IX. Foil-wrapped cultures were incubated semiaerobically for 3 days, and cells were harvested by centrifugation.

For inhibition of the conversion of divinyl protochlorophyllide to monovinyl protochlorophyllide and chlorophyllide, wild type and *bchD* cultures were grown semiaerobically to $A_{650} = 1.0$, and filter-sterilized nicotinamide (Sigma-Aldrich) dissolved in distilled H_2O was added to a final concentration of 12 mM (31). Control cultures had the same volume of distilled H_2O added but lacked nicotinamide. Cultures were incubated semiaerobically, and cells were harvested by centrifugation 33 h later (32).

Isolation and Identification of BChl Pathway Intermediates—For separation of metalloprotoporphyrins IX and their monomethyl esters, ether extracts of cells were filtered through a 0.2-μm filter, and pigments were separated by HPLC in a monomeric C18 column (Vydac). Pigments were eluted from the column using a 0.8 ml/min flow rate and a linear gradient changing from 80% solvent A (0.1 M ammonium acetate, pH 5.2), 20% solvent B (90% methanol, 0.1 M ammonium acetate, pH 5.2 (adjusted with glacial acetic acid)) to 100% solvent B over 10 min (26). The elution of peaks was monitored fluorometrically (excitation 420 nm; emission 595 nm), and pigments were identified using Mg-PPIX (Frontier Scientific) and Zn-PPIX (Sigma-Aldrich) standards.

For separation of divinyl protochlorophyllides, the hexane-extracted, acetone residue layer from cells treated with nicotinamide was filtered through a 0.2-μm filter and separated by HPLC in a Luna C18(2) column (Phenomenex). Pigments were eluted from the column as described above, except with a solvent gradient duration of 3 min. The elution of peaks was monitored by measuring absorbance at 440 nm, and pigments were identified by comparison of absorption spectra with values in the literature (31).

Mass spectrometry of HPLC-purified peaks was performed at the University of British Columbia microanalysis and mass spectrometry facility using a biflex IV MALDI-TOF mass spectrometer (Bruker). Briefly, the sample and trans-2-[3-(4-*tert*-butylphenyl)-2-methyl-2-propenylidene]malononitrile matrix were dissolved in dichloromethane, and 1 μl was applied to the target and dried in air. The sample was run using the reflector mode and pulsed ion extraction. Analysis of results was aided by Isotope Pattern Calculator version 4.0 (J. Yan).

Absorption and Fluorescence Spectroscopy and Quantification of Porphyrins—Fluorescence spectra were captured on a Varian Eclipse fluorescence spectrophotometer using 5–10-nm excitation and emission slit widths, medium photomultiplier tube setting, autofilters, and 600-nm/min scan speed. Analysis of spectra was performed using the Eclipse scan application and Microsoft Excel.

The quantification of Mg-PPIX and Zn-PPIX from hexane-extracted, acetone residue extractions of cells was based on fluorescence emission spectra from 575 to 700 nm with excitation at 420 nm. The concentrations of metalloprotoporphyrins IX were determined by comparison of 595-nm (Mg-PPIX) and 589-nm (Zn-PPIX) peak heights with a curve constructed using authentic standards in the same solvent.

PPIX was quantified using an established spectral deconvolution method (29). Hexane-extracted acetone residue samples were analyzed using fluorescence emission from 575 to 700 nm with excitation at 400 and 440 nm. Fluorescence emission due only to PPIX was determined through the deconvolution equation, which removes the contributions of other fluorescent species. The resulting deconvoluted emission intensity at 633 nm was compared with a standard curve constructed from authentic PPIX (Sigma-Aldrich) in the same solvent.

Quantification of divinyl protochlorophyllide fluorescence was done using an established spectral deconvolution method (29). Hexane-extracted, acetone residue samples were analyzed using fluorescence emission from 575 to 700 nm with excitation at 400 and 440 nm. Fluorescence emission due only to divinyl protochlorophyllide was determined through a deconvolution formula that removes the contributions of other fluorescent species from the fluorescence intensity of divinyl-Mg-protochlorophyllide in the wild type (excitation 440 nm; emission 638 nm) or divinyl-Zn-protochlorophyllide in the *bchD* mutant (excitation 440 nm; emission 634 nm).

Quantification of heme extracted from cells was performed using a chemiluminescent heme assay (34) because this method is resistant to interference from Zn-PPIX. Amounts of BChls were determined by absorption spectroscopy of acetone/methanol (7:2, v/v) extracts of purified membranes of known protein
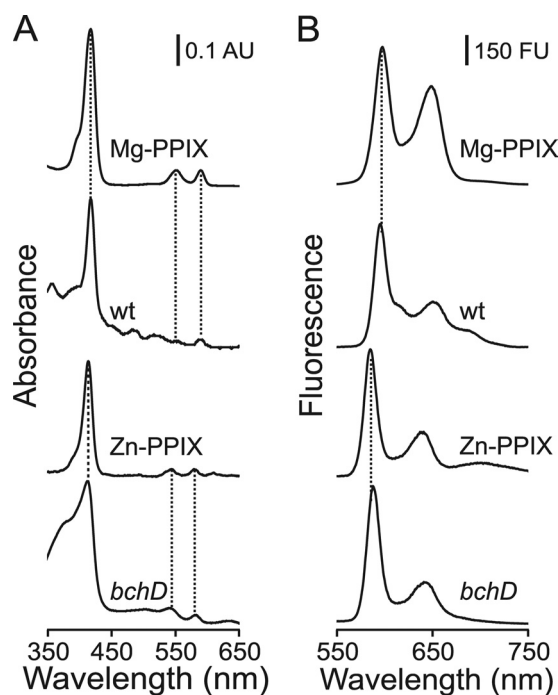

FIGURE 1. **Extracts of wild type cells contain Mg-protoporphyrin IX, whereas *bchD* mutant extracts contain Zn-protoporphyrin IX.** *A*, absorption spectra of extracts and authentic standards in ether. *B*, fluorescence emission spectra of extracts and authentic standards in ether, excitation at 420 nm. The *dotted lines* highlight peaks with similar wavelength maxima between spectra. *AU*, absorbance units; *FU*, fluorescence units.

amount, using $\epsilon = 75$ mM^{-1} cm^{-1} at 775 nm (Mg-BChl) and $\epsilon = 56.3$ mM^{-1} cm^{-1} at 771 nm (Zn-BChl) (35).

RESULTS

Analysis of Porphyrins in the Wild Type and bchD Mutant Strains—Previously, it had been speculated that Zn-PPIX is a precursor of Zn-BChl in the *R. sphaeroides bchD* mutant (25). Because only Mg-PPIX, never Zn-PPIX, had been detected in wild type *R. sphaeroides* and *A. rubrum* cells (26), discovering this metabolite in the *bchD* mutant would lend support to a zinc-early model of this Zn-BChl pathway.

To determine which metabolite is present in the *bchD* mutant, metalloporphyrins extracted from wild type and *bchD* cells were analyzed by absorption and fluorescence spectroscopy, relative to authentic Mg- and Zn-PPIX standards. Absorption spectroscopy revealed that the wild type extract exhibited a major peak at 418 nm along with smaller 553 and 590 nm peaks (Fig. 1*A*). These three peaks matched closely to those of authentic Mg-PPIX standard (418, 551, and 590 nm). The absorption spectrum of the extract of the *bchD* mutant strain exhibited a large peak at 414 nm as well as smaller peaks at 543 and 582 nm (Fig. 1*A*). The absorption peaks from the *bchD* mutant extract were similar to but blue-shifted relative to both the wild type strain extract and the Mg-PPIX standard. Instead, the peaks corresponded well to those of authentic Zn-PPIX (414, 544, and 580 nm) (Fig. 1*A*). Because of the different spectral signature of the *bchD* mutant extract compared with the wild type strain and authentic Mg-PPIX and the similarity to authentic Zn-PPIX, it appeared that the *bchD* mutant contained Zn-PPIX instead of Mg-PPIX. Fluorescence emission
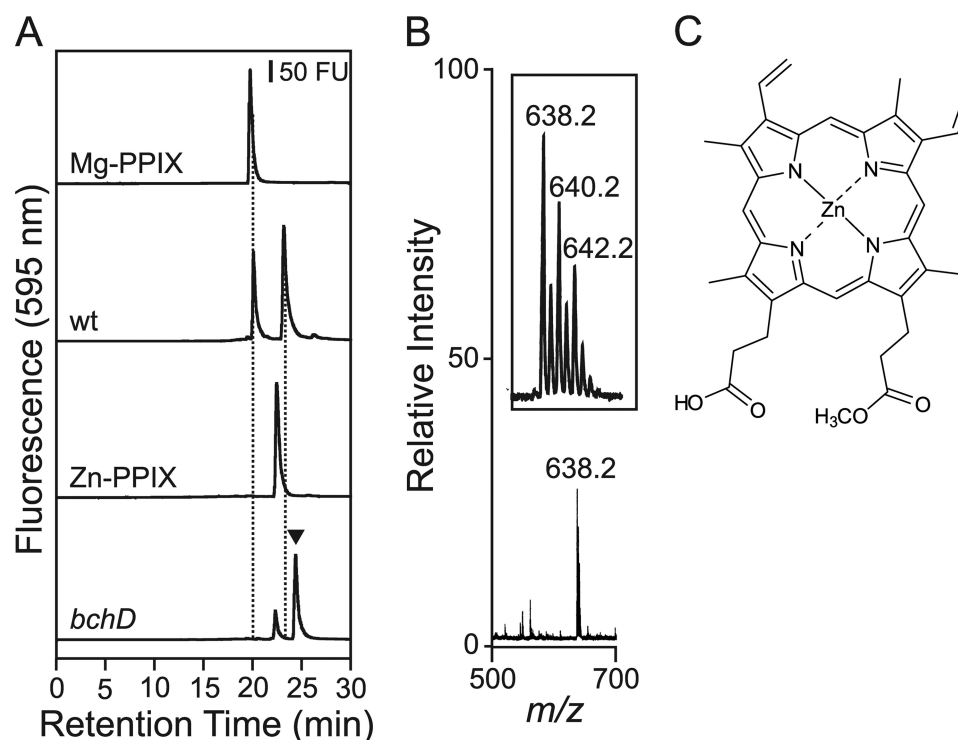
FIGURE 2. **Isolation and identification of Zn-protoporphyrin IX monomethyl ester from the *bchD* mutant.** *A*, HPLC separation of wild type and *bchD* mutant ether extracts and metalloprotoporphyrin IX standards. The *dotted lines* indicate retention time of Mg-protoporphyrin IX and Mg-protoporphyrin IX monomethyl ester from the wild type. ▼, peak collected for mass spectrometry. *B*, mass spectrum of substance in peak collected from *bchD* mutant extract. *Inset*, expanded view of the region around the *m/z* 638.2 peak. *C*, proposed structure of the *m/z* 638.2 substance, zinc protoporphyrin IX monomethyl ester. *FU*, fluorescence units.

spectra provided additional evidence that the *bchD* mutant extract contained Zn-PPIX. The wild type extracts had a major peak at 595 nm, which closely matched that of authentic Mg-PPIX (596 nm), whereas the *bchD* mutant peak at 589 nm is more similar to that of Zn-PPIX (588 nm) (Fig. 1*B*).

Together, the absorption and fluorescence emission data indicate that the *bchD* mutant synthesizes Zn-PPIX instead of Mg-PPIX. To confirm that the Zn^{2+} in Zn-BChl arises from Zn-PPIX, we searched for additional BChl biosynthetic intermediates in the *bchD* mutant.

Isolation and Identification of Zinc Protoporphyrin IX Monomethyl Ester—The second step of the wild type BChl biosynthetic pathway, following the Mg-chelatase, is the *S*-adenosylmethionine-dependent methylation of the ring III propionate of Mg-PPIX by the BchM enzyme (36). BchM is a cytoplasmic membrane-associated enzyme, and the product of the reaction is magnesium protoporphyrin IX monomethyl ester (Mg-PPIX-MME). Determination of the equivalent metabolite in the *bchD* mutant would help us define the beginning of the Zn-BChl pathway.

Extracts of wild type and *bchD* mutant cells were separated on HPLC, and the identities of metalloporphyrins were established by comparison with authentic standards. The results of this analysis showed that the wild type strain contained both Mg-PPIX and a metalloporphyrin with a 3-min longer retention time (Fig. 2*A*). The longer-retained substance has been shown by others to be Mg-PPIX-MME (26). Two metabolites were found in *bchD* mutant extracts, one with a retention time that matched that of Zn-PPIX, confirming the presence of this

substance, and a second with a 2-min longer retention time (Fig. 2*A*).

The material with the 2-min longer retention time in *bchD* extracts was isolated and subjected to MALDI-TOF mass spectrometry, revealing a peak at *m/z* 638.2 (Fig. 2*B*) that corresponds to the predicted mass of zinc protoporphyrin IX monomethyl ester (Zn-PPIX-MME). Additional evidence for the identity of this molecule came from the isotopic splitting pattern of the 638.2 *m/z* peak (Fig. 2*B*, *inset*), which matched that of a zinc-containing rather than a magnesium-containing molecule.

The combination of relative HPLC retention time, *m/z* value, and isotopic pattern of the isolated material led us to conclude that the material isolated from the *bchD* mutant was Zn-PPIX-MME. The proposed structure of this compound is shown in Fig. 2*C*. To the best of our knowledge, this is the first report of Zn-PPIX-MME identified in an organism.

Isolation and Identification of Divinyl-Zn-Protochlorophyllide—To further confirm the zinc-early hypothesis of Zn-BChl biosynthesis in the *bchD* mutant, we attempted to isolate the metabolite in this strain equivalent to the third intermediate of the wild type BChl biosynthetic pathway, divinyl magnesium protochlorophyllide (DV-Mg-PChlide). To increase the amount of this metabolite in cells, cultures were treated with nicotinamide, an inhibitor of the conversion of DV-Mg-PChlide to monovinyl magnesium protochlorophyllide (MV-Mg-PChlide). Previously, wild type *R. sphaeroides* cultures treated with this inhibitor were found to accumulate mainly DV-Mg-PChlide (31, 32).
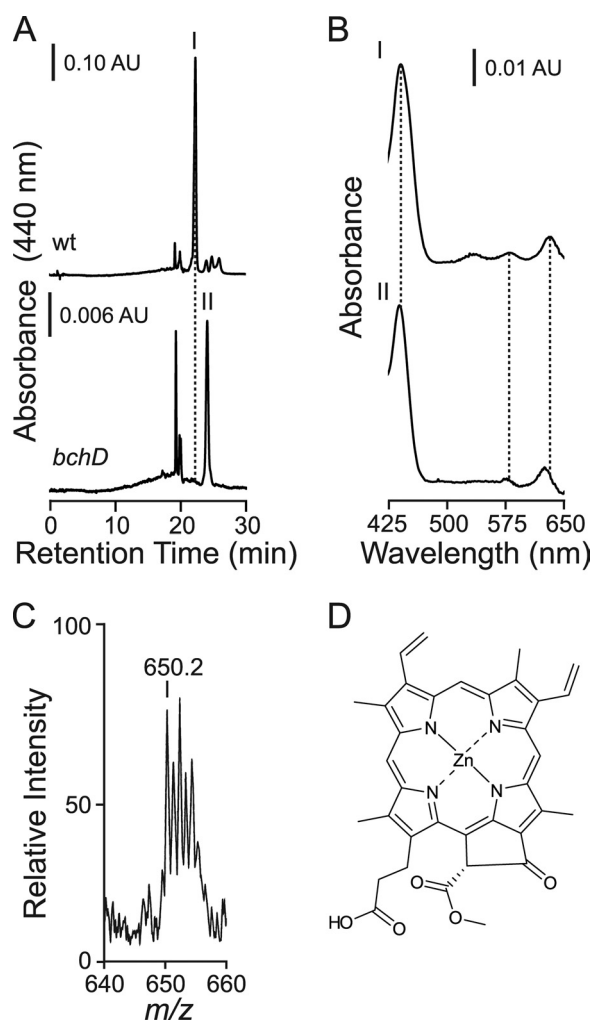
FIGURE 3. **Isolation and identification of divinyl-Zn-protochlorophyllide from nicotinamide-treated *bchD* mutant cells.** *A*, HPLC separation of wild type and *bchD* mutant cell extracts. The *dotted line* indicates the retention time of the divinyl-Mg-protochlorophyllide peak in the wild type sample. Peaks I and II were used for absorption spectroscopy. *B*, absorption spectra of substances in peaks I and II in methanol. The *dotted lines* indicate peak I (divinyl-Mg-protochlorophyllide) maxima at 441, 579, and 630 nm. Maxima for peak II were 438, 575, and 624 nm. *C*, mass spectrum of substance in peak II. *D*, proposed structure of *m/z* 650.2 substance in peak II, divinyl-Zn-protochlorophyllide. *AU*, absorbance units.

Extracts of the wild type and *bchD* mutant cells were analyzed by HPLC and monitored at 440 nm, the strongest absorption peak of DV-Mg-PChlide. The wild type HPLC trace showed one major species with a retention time of 22 min (peak I) (Fig. 3*A*). The absorption spectrum of this fraction matched that of DV-Mg-PChlide reported in the literature (31), with peaks at 441, 579, and 630 nm (Fig. 3*B*). The *bchD* mutant extract yielded two major peaks eluting at 19 and 24 min (Fig. 3*A*). The absorption spectrum of the 19 min peak matched that of PPIX with peaks at 398, 504, and 629 nm (data not shown). The 24 min peak (peak II) had an absorption spectrum similar to that of DV-Mg-PChlide but with blue-shifted peaks at 438, 575, and 624 nm (Fig. 3*B*).

Material from the 24 min HPLC peak of the *bchD* mutant extract (peak II) was collected and subjected to mass spectrometry, and a peak with mass of 650.2 *m/z* was observed (Fig. 3*C*), consistent with the predicted mass of 650.2 for divinyl-Zn-

protochlorophyllide (DV-Zn-PChlide). The isotopic pattern of this substance also indicated a zinc-containing molecule. Taking into account the HPLC retention time, blue-shifted spectral peaks, and the *m/z* data, we propose that the material of peak II is DV-Zn-PChlide (Fig. 3*D*). To the best of our knowledge, this is the first report of the identification of DV-Zn-PChlide produced by an organism. With the weight of evidence pointing to a novel zinc-early mechanism of Zn-BChl biosynthesis in the *bchD* mutant, we next turned to the question of how the first metabolite of the pathway is synthesized.

Role of Ferrochelatase in Zn-PPIX and Zn-BChl Biosynthesis—Early work using purified photosynthetic membranes from *R. sphaeroides* uncovered an enzymatic Zn-chelatase activity that was later ascribed to ferrochelatase (37), and it was subsequently shown that the *R. sphaeroides* ferrochelatase catalyzes both Zn^{2+} and Fe^{2+} chelation (38, 39). To evaluate the involvement of ferrochelatase in the production of Zn-PPIX and Zn-BChl in the *bchD* mutant, we used the inhibitor *N*-methylprotoporphyrin IX (NMPP). This inhibitor acts as a transition state analog of heme and competitively inhibits the *R. sphaeroides* ferrochelatase (40).

Wild type and *bchD* cultures were grown with high aeration so that cells were replete with heme but contained little or no BChl. The cultures were then shifted to semiaerobic growth to induce BChl production, with the simultaneous addition of NMPP of varying concentrations. After 3 days of growth, cells were harvested, and the amounts of Mg-PPIX and Mg-BChl in the wild type and of Zn-PPIX and Zn-BChl in the *bchD* mutant were determined. The amount of PPIX and heme in both the wild type and *bchD* strains was also measured.

In the wild type strain, Mg-BChl amounts increased upon treatment with NMPP up to 1.7-fold relative to untreated levels (Fig. 4*A*). In contrast, the Zn-BChl levels in the *bchD* mutant responded to ferrochelatase inhibition in a manner opposite to that seen for Mg-BChl in the wild type strain. The levels of Zn-BChl in the *bchD* mutant decreased with increasing concentrations of NMPP, down to 0.1-fold that of untreated cells (Fig. 4*A*). The effect of NMPP on the levels of Mg- and Zn-PPIX was very similar to the effect on Mg- and Zn-BChl in the respective strain (Fig. 4*B*). The amount of Mg-PPIX in the wild type strain when treated with 2.0 μM NMPP was increased 2.4-fold relative to the level in untreated cells, whereas the amount of Zn-PPIX in the *bchD* mutant at the same concentration of NMPP was reduced to 0.2-fold the untreated level. These results indicate that ferrochelatase inhibition in the *bchD* mutant has a marked inhibitory effect on the formation of both the first intermediate and the final product of the Zn-BChl pathway. In contrast, the effect on the analogous metabolites in the wild type was stimulatory. Therefore, it appears that ferrochelatase is necessary for the biosynthesis of Zn-BChl but not Mg-BChl.

The changes in PPIX levels caused by NMPP treatment showed a relationship between the wild type and *bchD* mutant strain different from that for metalloprotoporphyrin IX or BChl, but reinforced the difference between the two porphyrin pathways. The amount of PPIX in the wild type strain increased 2.7-fold at 2.0 μM NMPP, similar to the increases seen for Mg-BChl and Mg-PPIX levels upon treatment of cultures with this
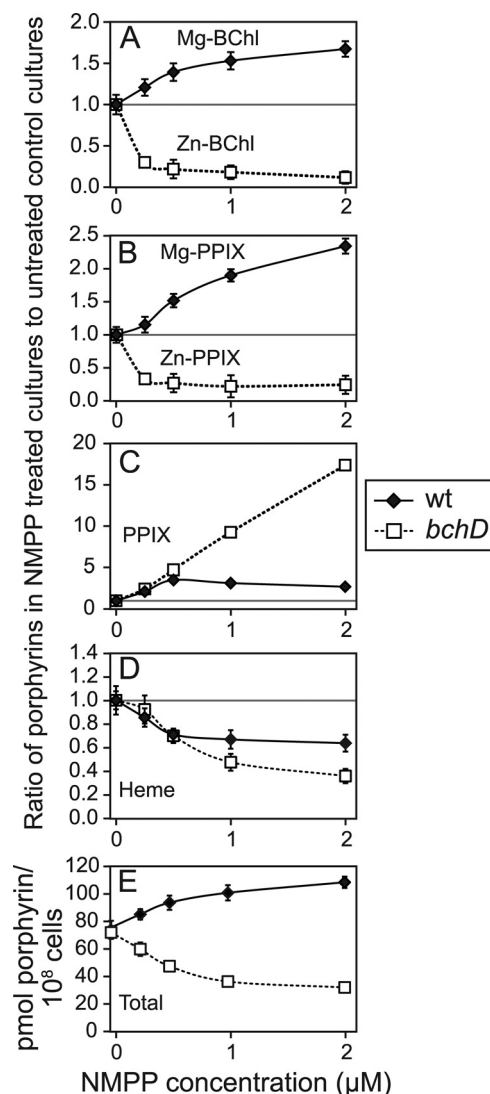
FIGURE 4. **Effect of ferrochelatase inhibition on metabolite levels in the wild type and *bchD* mutant strains.** Aerobic cultures were grown until A_{650} = 1.0 and diluted to A_{650} = 0.2 with fresh medium, and NMPP was added to various concentrations. Semiaerobic growth was continued for 3 days in the dark, and cultures were harvested and extracted. PPIX and metalloporphyrins were measured by fluorescence, BChls by absorption spectroscopy, and heme by chemiluminescence. Values on *vertical axes* (*A–D*) are ratios of porphyrins in NMPP-treated *versus* untreated cells, and the *horizontal axes* give the concentrations of NMPP inhibitor used. The *horizontal lines* (*A–D*) denote 1:1 ratios. *Points above* the *line* indicate cellular concentrations that increase upon ferrochelatase inhibition, and *points below* the *line* denote decreased cellular levels upon ferrochelatase inhibition. *Error bars*, S.D. (*n* = 3–4). *A*, Mg- and Zn-BChls. *B*, Mg- and Zn-metalloprotoporphyrins IX. *C*, PPIX. *D*, heme. *E*, total porphyrins, expressed as the molar sum of the porphyrins measured in *A–D*.

inhibitor (Fig. 4*C*). However, the PPIX level in the *bchD* mutant increased 18-fold in response to 2.0 μM NMPP (Fig. 4*C*), in stark contrast to the changes in the amounts of Zn-BChl and Zn-PPIX, in terms of both magnitude and direction of change.

Heme levels declined in both the wild type and *bchD* mutant strains treated with NMPP. The wild type levels decreased to 0.65-fold that of untreated cells, whereas the *bchD* mutant showed a larger decrease, down to 0.37-fold that of untreated cells (Fig. 4*D*). The cellular decrease in heme is thought to be due to the combined effect of inhibition of new heme synthesis
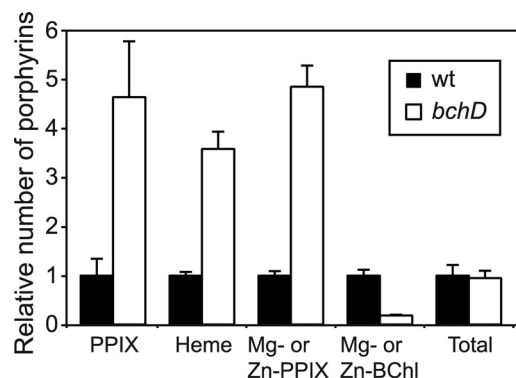

FIGURE 5. **Relative porphyrin levels in the wild type and *bchD* mutant strains.** Cultures were grown until mid-log phase, cells were harvested, and pigments were extracted. PPIX and metalloporphyrins were measured by fluorescence, BChls by absorption spectroscopy, and heme by chemiluminescence. Measurements of porphyrin molar concentrations in extracts of equal numbers of cells of each strain were normalized by dividing by the wild type values. *Error bars*, S.D. (*n* = 3–4).

and dilution of the heme pool present in the culture inoculum by cell growth and division.

The molar sum of all of the porphyrins measured in this inhibition experiment showed an interesting difference in trend between the wild type and *bchD* mutant strains with increasing concentrations of NMPP. Although the concentrations of total measured porphyrins in the wild type and *bchD* mutant were the same in the absence of NMPP, at 2 μM NMPP, the *bchD* mutant had a level 0.27-fold that of wild type (Fig. 4*E*). This effect was due to a combination of the wild type level increasing and the *bchD* mutant level decreasing as the NMPP concentration increased. To further investigate the porphyrin distribution in wild type and *bchD* mutant pathways in the normal state, we analyzed the relative amounts of several key types of porphyrins in more detail below.

Porphyrin Levels in the Wild Type and bchD Mutant Strains— After discovering that in the *bchD* mutant, ferrochelatase is the likely source of Zn-PPIX and that PPIX levels are highly dependent on the activity of this enzyme, we quantitatively determined the relative porphyrin metabolite concentrations in both strains. It was found that the *bchD* mutant contained 4.6-fold more PPIX per cell than the wild type strain (Fig. 5). The same relationship held true to a lesser extent for heme, which was 3.6-fold more abundant in the *bchD* mutant, and there was 4.9-fold more Zn-PPIX in the *bchD* mutant compared with Mg-PPIX in the wild type strain. However, the metabolite concentrations of the final product of the BChl pathway showed an opposite relationship to the early metabolites; the *bchD* mutant contained Zn-BChl at a level only 0.2-fold that of wild type Mg-BChl.

When all of these measured porphyrin metabolite concentrations were added up, the wild type and *bchD* mutant porphyrin levels were remarkably similar, with the *bchD* mutant having 96% of the wild type level (Fig. 5). This result indicates that although the total amounts of measured porphyrins in the BChl and heme pathways are the same in the two strains, the porphyrins in the *bchD* mutant are redistributed to the early parts of the pathway. The pattern of metabolite levels observed in the *bchD* mutant pointed to multiple steps limiting the Zn-BChl
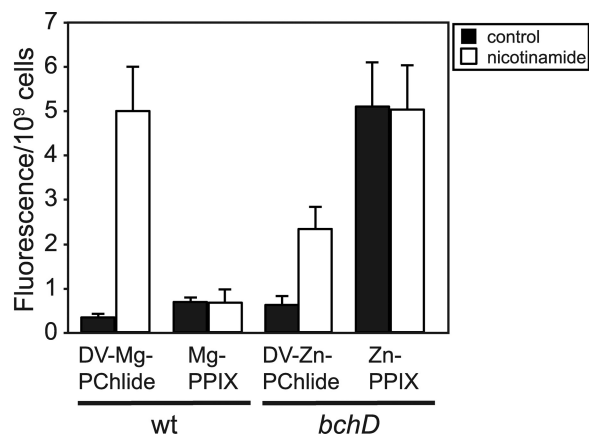
FIGURE 6. **Alterations in DV-PChlide and metalloprotoporphyrin IX levels caused by nicotinamide treatment of the wild type and *bchD* mutant strains.** Semiaerobic cultures were grown until $A_{650} = 1.0$, water or nicotinamide (12 mM) was added, and semiaerobic growth continued for 33 h. Extracts of cells were scanned using a fluorescence spectrophotometer, and deconvoluted emission at 638 nm (DV-Mg-PChlide) or 634 nm (DV-Zn-PChlide) was measured; Mg-PPIX and Zn-PPIX fluorescence was obtained from excitation at 420 nm and emission at 595 and 588 nm, respectively. *Error bars*, S.D. ($n = 3$–4).

pathway, choking off the production of Zn-BChl and causing early intermediates to build up.

To further delineate locations of pathway bottlenecks, we again used nicotinamide to inhibit the conversion of DV-PChlide to MV-PChlide to probe how much DV-PChlide concentrations changed when an artificial blockage in this step was introduced to the pathway. As shown in Fig. 6, the addition of nicotinamide caused a 15-fold increase in DV-Mg-PChlide fluorescence in wild type cultures, whereas there was only a 3.8-fold increase in DV-Zn-PChlide fluorescence in *bchD* mutant cultures. Previously, DV-Mg-PChlide has been observed excreted from cells (31), but we limited our analysis to intracellular concentrations of this metabolite.

The buildup of DV-PChlide seems to be confined to the step just prior to the inhibition because there was no detectable increase in Mg-PPIX fluorescence in wild type or Zn-PPIX fluorescence in the *bchD* mutant cultures when nicotinamide was added (Fig. 6). This result indicates that in the 33-h period during which conversion of DV-PChlide to MV-PChlide was inhibited by nicotinamide, more material was moving through the pathway and accumulating in the wild type strain than in the *bchD* mutant.

DISCUSSION

Previous work has established that the *bchD* mutant is unable to grow photosynthetically (24), produces Zn-BChl but neither Mg-BChl nor bacteriopheophytin *a*, and assembles light-harvesting and reaction center complexes containing Zn-BChl (25). Building on these prior results, the aims of the current work were 2-fold: 1) to elucidate the Zn-BChl biosynthetic pathway in the *bchD* mutant and 2) to explore why this pathway produces so little Zn-BChl relative to the amount of Mg-BChl produced in the wild type strain.

In this paper, the data indicate that the production of Zn-PPIX and Zn-BChl requires the ferrochelatase enzyme, and we identify the first three metabolic intermediates of the Zn-BChl

biosynthetic pathway as Zn-PPIX, Zn-PPIX-MME, and DV-Zn-PChlide. Furthermore, determination of the concentration of pathway intermediates in the *bchD* mutant revealed large amounts of intermediates early in the pathway, whereas low amounts of the Zn-BChl end product were found, indicating that a bottleneck exists in the pathway.

The Zn-BChl Biosynthetic Pathway in the bchD Mutant Begins with Zn-PPIX and Proceeds through a Zinc-early Mechanism Catalyzed by Ferrochelatase—Our discovery of a Zn-PPIX pool along with the isolation and identification of two zinc-containing intermediates from the beginning of the BChl biosynthetic pathway indicate that a zinc-early mechanism operates in the *bchD* mutant. This finding differentiates the pathway of Zn-BChl synthesis in the *R. sphaeroides bchD* mutant from that of *A. rubrum* and *Parachlorella kessleri*, which 1) possess a functional Mg-chelatase; 2) use a (B)Phe intermediate as substrate for Zn^{2+} chelation; 3) utilize a Zn^{2+} chelation reaction aided by acidic culture conditions that drive Zn^{2+} into (B)Phe; and 4) do not produce any zinc-containing intermediates (26, 27, 41). None of the conditions under which Zn-(B)Chl is produced in other organisms are present in *bchD* mutant cultures, which synthesize Zn-BChl without first producing Mg-BChl or bacteriopheophytin *a*, grow at neutral pH (where Zn^{2+} is less soluble), and appear to utilize Zn^{2+} as a physiological substrate.

Evidence for ferrochelatase as the first enzyme of the Zn-BChl pathway in the *bchD* mutant comes mainly from the NMPP inhibition experiments, consistent with earlier work showing that *R. sphaeroides* ferrochelatase has the ability to utilize Zn^{2+} as well as Fe^{2+} although at lowered activity (42). We found that when ferrochelatase was inhibited *in vivo*, the amounts of both the first and last metabolites in the Zn-BChl pathway were significantly decreased. The decrease in Zn-PPIX levels in the *bchD* mutant when ferrochelatase is inhibited is similar to what was seen in ALA-fed rat hepatocytes that produce Zn-PPIX (43). The addition of ALA, the precursor to PPIX, resulted in the production of excess PPIX and Zn-PPIX, but when the hepatocytes were also treated with NMPP, the levels of Zn-PPIX decreased, pointing to ferrochelatase as the source of Zn-PPIX (43). The similarity between the effect of NMPP on Zn-PPIX levels in rat hepatocytes and the *bchD* mutant indicates that the effect observed in these experiments is robust and consistent across phyla as well as pointing to ferrochelatase as the biological source of Zn-PPIX in the *bchD* mutant.

Although our experiments did not directly address the possibility that the BchHI subunits of the Mg-chelatase in the *bchD* mutant could somehow chelate Zn^{2+} into PPIX, the fundamental difference between the response of the wild type and *bchD* strains to ferrochelatase inhibition with NMPP makes this possibility unlikely (Fig. 4). If the BchHI subunits, instead of ferrochelatase, produced Zn-PPIX, then the levels of Zn-PPIX and Zn-BChl in the *bchD* mutant should have followed the same trend as Mg-PPIX and Mg-BChl levels in the wild type strain (Fig. 4, *A* and *B*). Instead, the effect was opposite, showing that the wild type Mg-chelatase is not inhibited by NMPP, whereas the enzyme responsible for Zn-PPIX and Zn-BChl production in the *bchD* mutant is inhibited by NMPP. Furthermore, exper-
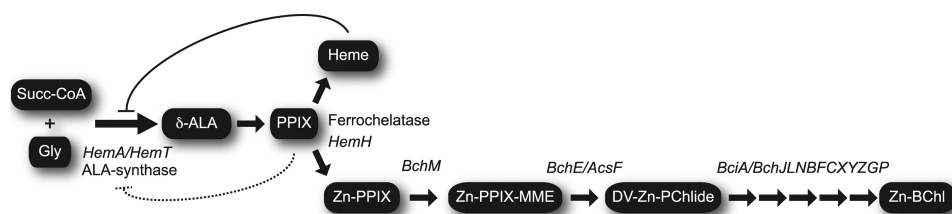
FIGURE 7. **Proposed biosynthetic pathway of Zn-BChl in the *bchD* mutant.** The *solid line* denotes negative feedback activity of heme on ALA synthase. The *dotted line* denotes proposed PPIX feedback on ALA synthase. Enzymes shown are as follows. *ALA-synthase*, δ-aminolevulinic synthase; *HemH*, ferrochelatase; *BchM*, *S*-Adenosylmethionine:magnesium protoporphyrin IX *O*-methyltransferase; *BchE* and *AcsF*, magnesium protoporphyrin IX monomethyl ester cyclases; *BciA* and *BchJ*, 8-vinyl reductase; *BchLNB*, protochlorophyllide reductase; *BchF*, 3-vinyl bacteriochlorophyllide *a* hydroxylase; *BchC*, 3-hydroxyethyl bacteriochlorophyllide *a* dehydrogenase; *BchXYZ*, chlorin reductase; *BchG*, bacteriochlorophyll synthase; *BchP*, geranylgeranyl reductase. Metabolites shown are as follows. *Succ-CoA*, succinyl-CoA; *Gly*, glycine; *δ-ALA*, δ-aminolevulinic acid; *PPIX*, protoporphyrin IX; *Zn-PPIX*, Zn-protoporphyrin IX; *Zn-PPIX-MME*, Zn-protoporphyrin IX monomethyl ester; *DV-Zn-PChlide*, divinyl-Zn-protochlorophyllide; *Zn-BChl*, Zn-bacteriochlorophyll *a*.

iments on the *R. sphaeroides bchHID* genes expressed in *E. coli* showed no Mg-chelatase activity or production of Zn-PPIX in the absence of the *bchD* gene product (17). Although this observation is not proof, it provides evidence that the Mg-chelatase BchHI subunits are unlikely to carry out the observed Zn^{2+} chelation. Moreover, Zn-PPIX has been observed in organisms such as yeast, rats, and humans (43–45), all of which possess a ferrochelatase but no Mg-chelatase, consistent with the idea that ferrochelatase is the source of Zn-PPIX in the *bchD* mutant.

Evidence for the ability of BChl pathway enzymes downstream of Mg-chelatase, such as BchM and BchE, to accept zinc-containing substrates, comes from our identification of Zn-PPIX-MME and DV-Zn-PChlide in the *bchD* mutant (Figs. 2 and 3). Additionally, studies of several enzymes from the chlorophyll anabolic and catabolic pathways were shown to utilize zinc-containing substrates with similar efficiency to magnesium-containing substrates (46–49).

Based on strong support coming from several different lines of evidence in this work, we propose a model of a novel variant of Zn-BChl biosynthesis operating in the *bchD* mutant (Fig. 7). This variant pathway utilizes ferrochelatase in place of Mg-chelatase to add a Zn^{2+} to PPIX, forming Zn-PPIX. This Zn-PPIX then proceeds through the otherwise native BChl biosynthetic pathway, producing Zn-BChl.

Distribution of Metabolites and Regulation of the Zn-BChl Pathway—Overall, the total amount of measured porphyrins in the *bchD* mutant pathway was equivalent to that found in the wild type pathway, but, in contrast to the wild type strain, the early BChl biosynthetic intermediates in the *bchD* mutant are at higher levels than the (Zn-)BChl end product (Fig. 5). Although it is known that heme is a negative feedback signal that regulates ALA synthase (13, 50), leading to a prediction that higher heme levels should result in lowered amounts of other porphyrins, experiments on other Mg-chelatase mutants indicate that this model is too simplistic. Higher than normal levels of both heme and PPIX were seen in a *Chlamydomonas* strain with a knock-out in a gene encoding a homolog of the BchH Mg-chelatase subunit (51), and *Rhodobacter capsulatus bchH*, *bchD*, and *bchI* mutants all accumulated PPIX, although heme levels were not measured (52, 53).

Measurement of the total amount of porphyrins in the wild type and *bchD* mutant strains in the ferrochelatase inhibition experiment sheds light on additional regulatory mechanisms of porphyrin pathways in *R. sphaeroides*. The decline in heme levels in both strains due to the action of the NMPP (Fig. 4D) would have signaled ALA synthase to *increase* flux through the pathway, increasing porphyrin production (12, 13). The wild type strain used Mg-chelatase to convert PPIX to Mg-PPIX and Mg-BChl, keeping PPIX levels from increasing beyond 2-fold above uninhibited levels (Fig. 4C) at 2 μM NMPP, but in the process increasing the sum of all measured porphyrins 1.5-fold. In contrast to the wild type, the *bchD* mutant had a 0.4-fold decrease in the total amount of measured porphyrins as NMPP concentration increased (Fig. 4E). Contributing to this decrease were lowered levels of Zn-BChl, Zn-PPIX, and heme, whereas PPIX production, which does not depend on ferrochelatase, increased nearly 7-fold more than the increase seen in the wild type strain. The increases in PPIX levels in the *bchD* mutant, although large, did not fully compensate for the decreases in other metabolite levels, so we speculate that there is a signal in the *bchD* mutant that modulates ALA synthase activity in addition to the signal from lowered heme levels. This signal in the *bchD* mutant decreased the flux through the pathway from ALA to PPIX in cells exposed to the inhibitor NMPP, causing a decrease in total porphyrins from uninhibited levels (Fig. 4E). Based on the limited number of metabolites measured here, the likely candidate for this negative regulation is PPIX (Fig. 7), which was the sole intermediate in the *bchD* mutant that increased in the ferrochelatase inhibition experiments (Fig. 4C).

The elevated levels of early BChl biosynthetic intermediates in the *bchD* mutant indicate a bottleneck in the pathway. The *bchD* mutant contains 3.6–4.9-fold more PPIX, heme, and (Mg/Zn-)PPIX than the wild type strain, whereas the amount of Zn-BChl end product is only 0.2-fold that of wild type (Fig. 5). Using nicotinamide to probe the location of the bottleneck revealed only a 0.3-fold increase in DV-Zn-PChlide accumulation in the *bchD* mutant compared with wild type DV-Mg-PChlide accumulation (Fig. 6). This value closely mirrors the relative BChl levels between wild type and *bchD* mutant strains (Fig. 5), suggesting that a bottleneck in the pathway is upstream of the conversion of DV-PChlide to MV-PChlide.

The proposed Zn-BChl biosynthetic pathway in the *bchD* mutant is an example of a naturally occurring "mutasynthetic" pathway, where the elimination of a biosynthetic enzyme in a pathway (usually the first) is compensated for by

supplying an alternative substrate (54, 55). In general, this practice is used to feed cells an exogenous substrate to produce novel end products for drug discovery, but in this case, *R. sphaeroides* itself supplies the alternative substrate endogenously. Mutasynthetic pathways typically are limited by early substrate availabilities, whereas we found high levels of early substrates in the Zn-BChl pathway and lowered metabolite levels at later steps, although similar situations have been seen in metabolic engineering efforts using other organisms (56). The general principle learned from these efforts is the importance of matching enzyme levels with substrate levels so that inhibitory intermediates do not accumulate (57). It is possible that the same principle applies in the Zn-BChl pathway bottleneck in the *bchD* mutant; however, enzyme levels and affinity for zinc-containing substrates are currently unknown.

Evolutionary Significance of the Zn-BChl Biosynthetic Pathway—The structure and evolutionary origin of ferrochelatase and Mg-chelatase are very different despite catalyzing similar reactions. Ferrochelatase is a single subunit of 115 kDa (39), whereas Mg-chelatase is a 1.1–1.2-MDa complex consisting of 2–3 copies of BchH, 6 copies of BchI, and 6 copies of BchD (58). Although both enzymes are located in the cytoplasm, the ferrochelatase may be membrane-associated (17, 39). Both enzymes catalyze the insertion of a divalent cation, but ferrochelatase catalyzes the reaction in the absence of ATP (39), whereas Mg-chelatase requires ~15 ATPs per insertion event (59). Mg-chelatase is related to other AAA^+-chelatases, such as the aerobic cobaltochelatase formed by CobNST (60), whereas ferrochelatase is in a class of non-homologous chelatases that includes the anaerobic cobaltochelatases CbiK and CbiX (61).

Considering the many differences between these two enzymes, it is surprising that the loss of Mg-chelatase revealed a connection between ferrochelatase and the BChl biosynthetic pathway. This may be fortuitous, because of the similar cellular localization of these two chelatases and a relaxed substrate specificity of the BChl biosynthetic enzymes, or it could indicate a deeper association between heme and BChl biosynthesis. Is it possible that production of Zn-PPIX by ferrochelatase and subsequent entry into the BChl biosynthetic pathway reveal an ancestral pathway that functioned prior to the evolution of Mg-chelatase? The ancestor of all photosynthetic organisms has been proposed to have resembled a purple bacterium that lived in a reduced anaerobic environment containing Mg^{2+}, Fe^{2+}, and Zn^{2+} (62, 63). The relative abundance of these cations is highly dependent on pH, with acidic conditions favoring Zn^{2+} availability and neutral conditions favoring the loss of soluble Zn^{2+} as ZnS, $ZnCl_2$, and $Zn(OH_2)_2$ precipitates (64–66). It is interesting to speculate that a ferrochelatase in an ancestral organism produced both heme and Zn-PPIX due to the promiscuous nature of early enzymes (67). In light of the suggested evolutionary linkage of cytochrome *b* and the reaction center proteins in *Rhodobacter* (33), the use of a single enzyme to produce two cofactors would be a parsimonious way to embark on the development of a primitive light-driven electron transfer system.

REFERENCES

1. Niederman, R. A., Mallon, D. E., and Langan, J. J. (1976) *Biochim. Biophys. Acta* **440,** 429–447
2. Bauer, C. E., Setterdahl, A., Wu, J., and Robinson, B. R. (2009) in *The Purple Phototrophic Bacteria* (Hunter, C. N., Daldal, F., Thurnauer, M. C., and Beatty, J. T., eds) pp. 707–725, Springer, Dordrecht, The Netherlands
3. Braatsch, S., Gomelsky, M., Kuphal, S., and Klug, G. (2002) *Mol. Microbiol.* **45,** 827–836
4. Zeilstra-Ryalls, J. H., and Kaplan, S. (1995) *J. Bacteriol.* **177,** 6422–6431
5. Gomelsky, L., Moskvin, O. V., Stenzel, R. A., Jones, D. F., Donohue, T. J., and Gomelsky, M. (2008) *J. Bacteriol.* **190,** 8106–8114
6. Lascelles, J. (1968) *Biochem. Soc. Symp.* **28,** 49–59
7. Willows, R. D., and Kriegel, A. M. (2009) in *The purple phototrophic bacteria* (Hunter, C. N., Daldal, F., Thurnauer, M. C., and Beatty, J. T., eds) pp. 57–79, Springer, Dordrecht, The Netherlands
8. Tuboi, S., Kim, H. J., and Kikuchi, G. (1970) *Arch. Biochem. Biophys.* **138,** 155–159
9. Neidle, E. L., and Kaplan, S. (1993) *J. Bacteriol.* **175,** 2304–2313
10. Kikuchi, G., Shemin, D., and Bachmann, B. J. (1958) *Biochim. Biophys. Acta* **28,** 219–220
11. Pappas, C. T., Sram, J., Moskvin, O. V., Ivanov, P. S., Mackenzie, R. C., Choudhary, M., Land, M. L., Larimer, F. W., Kaplan, S., and Gomelsky, M. (2004) *J. Bacteriol.* **186,** 4748–4758
12. Yubisui, T., and Yoneyama, Y. (1972) *Arch. Biochem. Biophys.* **150,** 77–85
13. Burnham, B. F., and Lascelles, J. (1963) *Biochem. J.* **87,** 462–472
14. Barrett, J., and Jones, O. T. (1978) *Biochem. J.* **174,** 277–281
15. Kanazireva, E., and Biel, A. J. (1996) *Gene* **170,** 149–150
16. Jensen, P. E., Gibson, L. C., Henningsen, K. W., and Hunter, C. N. (1996) *J. Biol. Chem.* **271,** 16662–16667
17. Gibson, L. C., Willows, R. D., Kannangara, C. G., von Wettstein, D., and Hunter, C. N. (1995) *Proc. Natl. Acad. Sci. U.S.A.* **92,** 1941–1944
18. Kannangara, C. G., Vothknecht, U. C., Hansson, M., and von Wettstein, D. (1997) *Mol. Gen. Genet.* **254,** 85–92
19. Papenbrock, J., Gräfe, S., Kruse, E., Hänel, F., and Grimm, B. (1997) *Plant J.* **12,** 981–990
20. Sawicki, A., and Willows, R. D. (2008) *J. Biol. Chem.* **283,** 31294–31302
21. Fodje, M. N., Hansson, A., Hansson, M., Olsen, J. G., Gough, S., Willows, R. D., and Al-Karadaghi, S. (2001) *J. Mol. Biol.* **311,** 111–122
22. Bollivar, D. W. (2006) *Photosynth. Res.* **90,** 173–194
23. Willows, R. D. (2003) *Nat. Prod. Rep.* **20,** 327–341
24. Coomber, S. A., Chaudhri, M., Connor, A., Britton, G., and Hunter, C. N. (1990) *Mol. Microbiol.* **4,** 977–989
25. Jaschke, P. R., and Beatty, J. T. (2007) *Biochemistry* **46,** 12491–12500
26. Masuda, T., Inoue, K., Masuda, M., Nagayama, M., Tamaki, A., Ohta, H., Shimada, H., and Takamiya, K. I. (1999) *J. Biol. Chem.* **274,** 33594–33600
27. Wakao, N., Yokoi, N., Isoyama, N., Hiraishi, A., Shimada, K., Kobayashi, M., Kise, H., Iwaki, M., Itoh, S., Takaichi, S., and Sakurai, Y. (1996) *Plant Cell Physiol.* **37,** 889–893
28. Sambrook, J., Fritsch, E. F., and Maniatis, T. (1989) *Molecular Cloning: A Laboratory Manual*, 2nd ed., Cold Spring Harbor Laboratory Press, Cold Spring Harbor, NY
29. Rebeiz, C. A. (2002) in *Heme, Chlorophyll, and Bilins: Methods and Protocols* (Smith, A. G., and Witty, M., eds) pp. 111–155, Humana Press, Totowa, NJ
30. Stillman, L. C., and Gassman, M. L. (1978) *Anal. Biochem.* **91,** 166–172
31. Shioi, Y., Doi, M., and Böddi, B. (1988) *Arch. Biochem. Biophys.* **267,** 69–74
32. Gough, S. P., Petersen, B. O., and Duus, J. O. (2000) *Proc. Natl. Acad. Sci. U.S.A.* **97,** 6908–6913

33. Xiong, J., and Bauer, C. E. (2002) *J. Mol. Biol.* **322,** 1025–1037
34. Masuda, T., and Takahashi, S. (2006) *Anal. Biochem.* **355,** 307–309
35. Hartwich, G., Fiedor, L., Simonin, I., Cmiel, E., Schafer, W., Noy, D., Scherz, A., and Scheer, H. (1998) *J. Am. Chem. Soc.* **120,** 3675–3683
36. Gibson, L. C., and Hunter, C. N. (1994) *FEBS Lett.* **352,** 127–130
37. Wacker, W. E., Tait, G. H., and Neuberger, A. (1965) *Biochemistry* **4,** 940–942
38. Mazanowska, A. M., Neuberger, A., and Tait, G. H. (1966) *Biochem. J.* **98,** 117–127
39. Dailey, H. A. (1982) *J. Biol. Chem.* **257,** 14714–14718
40. Moody, M. D., and Dailey, H. A. (1985) *J. Bacteriol.* **161,** 1074–1079
41. Ikegami, I., Nemoto, A., and Sakashita, K. (2005) *Plant Cell Physiol.* **46,** 729–735
42. Jones, M. S., and Jones, O. T. (1970) *Biochem. J.* **119,** 453–462
43. Jacobs, J. M., Sinclair, P. R., Sinclair, J. F., Gorman, N., Walton, H. S., Wood, S. G., and Nichols, C. (1998) *Toxicology* **125,** 95–105
44. Pretlow, T. P., and Sherman, F. (1967) *Biochim. Biophys. Acta* **148,** 629–644
45. Labbé, R. F., Vreman, H. J., and Stevenson, D. K. (1999) *Clin. Chem.* **45,** 2060–2072
46. Rüdiger, W., Böhm, S., Helfrich, M., Schulz, S., and Schoch, S. (2005) *Biochemistry* **44,** 10864–10872
47. Nasrulhaq-Boyce, A., Griffiths, W. T., and Jones, O. T. (1987) *Biochem. J.* **243,** 23–29
48. Scheumann, V., Helfrich, M., Schoch, S., and Rudiger, W. (1996) *Z. Naturforsch. C* **51,** 185–194
49. Scheumann, V., Ito, H., Tanaka, A., Schoch, S., and Rüdiger, W. (1996) *Eur. J. Biochem.* **242,** 163–170
50. Lascelles, J. (1960) *J. Gen. Microbiol.* **23,** 487–498
51. Chekounova, E., Voronetskaya, V., Papenbrock, J., Grimm, B., and Beck, C. F. (2001) *Mol. Genet. Genomics* **266,** 363–373
52. Bollivar, D. W., Suzuki, J. Y., Beatty, J. T., Dobrowolski, J. M., and Bauer, C. E. (1994) *J. Mol. Biol.* **237,** 622–640
53. Yang, Z. M., and Bauer, C. E. (1990) *J. Bacteriol.* **172,** 5001–5010
54. Wohlleben, W., and Pelzer, S. (2002) *Chem. Biol.* **9,** 1163–1164
55. Weissman, K. J. (2007) *Trends Biotechnol.* **25,** 139–142
56. Keasling, J. D. (2008) *ACS Chem. Biol.* **3,** 64–76
57. Martin, V. J., Pitera, D. J., Withers, S. T., Newman, J. D., and Keasling, J. D. (2003) *Nat. Biotechnol.* **21,** 796–802
58. Lundqvist, J., Elmlund, H., Wulff, R. P., Berglund, L., Elmlund, D., Emanuelsson, C., Hebert, H., Willows, R. D., Hansson, M., Lindahl, M., and Al-Karadaghi, S. (2010) *Structure* **18,** 354–365
59. Reid, J. D., and Hunter, C. N. (2004) *J. Biol. Chem.* **279,** 26893–26899
60. Lundqvist, J., Elmlund, D., Heldt, D., Deery, E., Söderberg, C. A., Hansson, M., Warren, M., and Al-Karadaghi, S. (2009) *J. Struct. Biol.* **167,** 227–234
61. Beck, R., Raux, E., Thermes, C., Rambach, A., and Warren, M. (1997) *Biochem. Soc. Trans.* **25,** 77S
62. Nisbet, E. G., Cann, J. R., and Vandover, C. L. (1995) *Nature* **373,** 479–480
63. Xiong, J., Fischer, W. M., Inoue, K., Nakahara, M., and Bauer, C. E. (2000) *Science* **289,** 1724–1730
64. Williams, R. J. (1997) *Cell. Mol. Life Sci.* **53,** 816–829
65. Lazcano, A., and Miller, S. L. (1996) *Cell* **85,** 793–798
66. Lide, D. R. (2009) in *CRC Handbook of Chemistry and Physics*, 90th Ed. (Lide, D. R., ed) pp. 8–123, CRC Press, Inc., Boca Raton, FL
67. Jensen, R. A. (1976) *Annu. Rev. Microbiol.* **30,** 409–425